

1 Security and Communication Networks

2 A novel TRNG based on traditional ADC non-linear effect and 3 chaotic map for IoT security and anti-collision

4 Gang Li,¹ Haoyang Sun,¹ Peiqi Wu,¹ Yuedan Zhou,¹ Xiaochuan Fang,² Zhenbing Li,¹ Jian
5 Li,¹ Yongjun Huang,¹ and Guangjun Wen,¹

6 ¹University of Electronic Science and Technology of China, Chengdu, China

7 ²Queen Mary University of London, London, United Kingdom

8 Guangjun Wen; wgj@uestc.edu.cn

9 Abstract

10 In the rapidly developing Internet of Things (IoT) applications, how to achieve rapid
11 identification of massive devices and secure the communication of wireless data based on
12 low cost and low power consumption is the key problem to be solved urgently. This paper
13 proposes a novel true random number generator (TRNG) based on ADC nonlinear effect and
14 chaotic map, which can be implemented by traditional processors with built-in ADCs, such as
15 MCU, DSP, ARM, and FPGA etc. The processor controls the ADC to sample the changing
16 input signal to obtain the digital signal D_{ADC} , and then extracts some bits of D_{ADC} to generate
17 the true random number (TRN). At the same time, after a delay based on D_{ADC} , the next time
18 ADC sampling is carried out, and the cycle continues until the processor stops generating the
19 TRN. Due to the nonlinear effect of ADC, the D_{ADC} obtained from each sampling is
20 stochastic, and the changing input signal will sharply change the delay time, thus changing
21 the sampling interval (called random interval sampling). As the input signal changes, D_{ADC}
22 with strong randomness is obtained. The whole operation of the TRNG resembles a chaotic
23 map, and this method also eliminates the pseudo-random property of chaotic map by
24 combining the variable input signal (including noise) with the nonlinear effect of ADC. The
25 simulation and actual test data are verified by NIST, and the verification results show that the
26 random numbers generated by the proposed method have strong randomness and can be used
27 to implement TRNG. The proposed TRNG has the advantages of low cost, low power
28 consumption and strong compatibility, and the rate of generating true random number is more
29 than 1.6 Mbps (determined by ADC sampling rate and processor frequency), which is very
30 suitable for IoT sensor devices for security encryption algorithms and anti-collision.

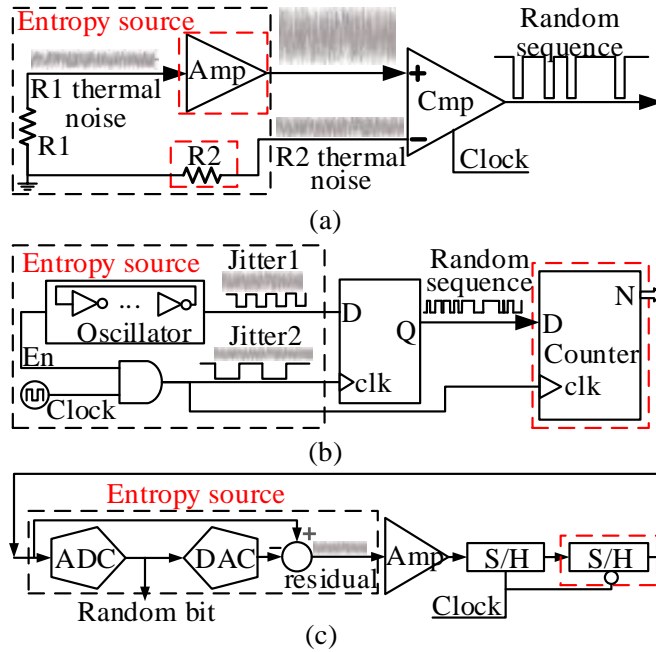
31 Introduction

32 In recent years, random numbers (RNs) have been widely used in the fields of encryption
33 algorithm, wireless communication, statistical analysis and radio frequency identification
34 (RFID) [1-10]. RNs can be divided into pseudo-random numbers (PRNs) [11] and true
35 random numbers (TRNs) [12]. PRNs are realized by deterministic algorithms, which have
36 periodic behaviors and can be completely repeated. Their randomness is determined by the
37 complexity and computational accuracy of the algorithm [13]. TRNs are often derived from
38 physical phenomena (such as thermal noise and scintillation noise) and realized by

39 combining certain algorithms and post-processing, which have truly unpredictable
 40 characteristics [14].

41 With the rapid development of IoT technology, wireless sensor networks (WSNs) have been
 42 deeply studied and widely applied in various fields [15-21]. Due to the explosive growth of
 43 wireless communication equipment, the communication security has attracted more and more
 44 attention [22,23]. It is known that the encryption algorithm can effectively improve the
 45 security performance of wireless communication system, and RNs play a very important role
 46 in the encryption algorithm [24]. Although PRNs do not require external circuits, as for
 47 deterministic algorithms, PRNs are very vulnerable to malicious attacks. Also, in WSNs,
 48 especially in wearable and implantable systems, the design of low-power and low-resource
 49 consuming structures is crucial because it can extend the longevity of batteries, or lengthen
 50 the distance of wireless communication between passive sensing nodes. To improve the
 51 security performance of the wireless communication in an effective method, it is obligatory
 52 to design a special true random number generator (TRNG) applied to sensing nodes.

53 The noise of analog circuit is used as the entropy source, making TRNG extremely
 54 susceptible to noise. According to the manifestation form of noise, the structure of TRNG can
 55 be divided into three categories, as shown in Fig. 1 : 1) Comparison structure based on
 56 thermal noise [25-27]; 2) Beat frequency detection (BFD) structure based on clock jitter [28-
 57 32]; 3) ADC residual recycling structure [33-39], also known as chaotic map. In Fig. 1, the
 58 red dotted part can be omitted.



59
 60 Fig. 1 Architecture of TRNG. (a) Comparing the noise, (b) beat frequency detect, (c) ADC chaotic map.

61 The noise comparison structure harvests the random information of the entropy source
 62 (resistance thermal noise) with comparators (equivalent to 1-bit ADC) and converts the noise
 63 signal into a random sequence. The noise must be amplified to a certain level to meet the
 64 accuracy requirements of the comparator/ADC. In order to make the amplified noise output
 65 as white as possible, a high-gain and wide-bandwidth amplifier is required. This amplifier has
 66 high power and cost, and it is not suitable for low power or low cost equipment.

67 The BFD structure harvests the random information of an entropy source (clock jitter noise of
68 an oscillator) with a register, which is a common method to realize TRNs. This method
69 requires the use of custom chip or Field Programmable Gate Array (FPGA) [40-44]. BFD is a
70 more reliable noise sampling technique compared to noise comparison. However, due to the
71 oscillator jitter is insufficient, the generated data is not random enough. Moreover, two
72 continuously oscillating clocks are energy engulfing, resulting in the increase of the power
73 consumption of the system. Furthermore, the structure also requires special chips or FPGA.
74 In other words, it not only increases the cost and power consumption of the system, but also
75 has finite applications, as it cannot be used in MCU, DSP, ARM and other traditional
76 microprocessors.

77 The ADC based on residual recycling structure takes the quantization error of the ADC as its
78 next input signal. After several iterations, the RNs of the ADC output show completely
79 different characteristics. This is exactly the property of chaotic map—A small change of the
80 input signal leads to an utterly distinctive output. Therefore, the structure based on ADC non-
81 linear chaotic map, which has been widely investigated, can be a desirous alternative for the
82 generation of TRNs. Literature [1] proposed the use of SAR ADC and dynamic residual
83 amplifiers to achieve TRNG. This method reduces the power consumption of the system
84 through selective activation of the fine-SAR ADC by coarse-SAR ADC. Literature [26]
85 proposed a method to realize TRNG by combining resistive thermal noise, oscillator
86 sampling and discrete time chaotic systems, and its performance is better than the TRNG
87 realized by these three methods alone. In [33-36], multiple ADCs were proposed to realize
88 TRNG using pipeline architecture. In each level, ADC used a resolution of 1.5-bits and the
89 residual signal output of the previous level becomes its new input. In literature [37], after the
90 completion of the SAR ADC, the comparator was used to continue to compare the lowest bit
91 (residual) of the ADC output once, and the comparison result was regarded as TRNs, so that
92 the analog-to-digital conversion function and the TRNG can be completed at the same time.
93 Pipeline ADC was also adopted in [2] in the realization of TRNG. Compared with [1,33-35],
94 a dynamic residual amplifier with a gain of less than 2 (1.9 for simulation) was used to avoid
95 system oscillation. In addition, the bit shuffling technique was employed to replace the shift
96 register so as to improve the statistical characteristics of the generated sequence.

97 The previously mentioned methods of realizing TRNG based on ADC chaotic map are
98 relatively complex to implement and requires special circuit structures. Its application for
99 dedicated chips complexes the design and increases the expense of the system. Literature [25]
100 introduces an approach to generate TRNs by the voltage value of ADC sampling resistance
101 divider circuit using traditional MCU. The approach relies unduly on the resistance and the
102 thermal noise of the circuit. If the thermal noise is low and the ADC precision is not high
103 enough, the ADC sampling output data shows slight or no changes, which makes it difficult
104 to generate TRNs. Fortunately, Literature [38,39] presents a method to realize TRNG using a
105 structure of combined traditional microprocessor and pipeline ADC. This is a typical example
106 of realizing TRNG based on ADC chaotic map with microprocessors (as shown in Fig. 1 (c)).
107 However, its structure is too complex to be used in low-power devices.

108 To solve the above problems, this paper proposes a novel method for TRNG based on ADC
109 nonlinear effect and chaotic map, which can be realized by either custom chips including
110 programmable logic devices with ADC, such as FPGA, etc. or traditional microprocessors
111 such as MCU, DSP, and ARM. A RC circuit and the sensor circuit with RC function are used
112 as the entropy source of TRNG. The processor controls the working state of the entropy
113 source circuit (on or off), so that the entropy source circuit can output varying voltage signal

114 V_{ADC} . The processor then controls the ADC to sample the V_{ADC} to obtain the digital signal
 115 D_{ADC} , which is used to generate TRNs. At the same time, the processor delays some time
 116 based on D_{ADC} , then it continues to control ADC to obtain D_{ADC} , and generate TRNs
 117 afterwards. This cycle goes on until enough TRNs are generated. Because of the randomness
 118 of circuit noise, D_{ADC} also has a certain randomness, and the nonlinear effect of ADC can
 119 further increase the randomness of D_{ADC} . These two factors add great uncertainty to the
 120 proposed TRNG. Furthermore, changing input voltage (excluding noise) makes D_{ADC} change
 121 as well, and therefore, the sampling interval of ADC also has randomness based on the delay
 122 of D_{ADC} . In short, because of the changing input voltage V_{ADC} , random interval sampling
 123 further improves the randomness of D_{ADC} . The circuit noise and the nonlinear effect of ADC
 124 are used as the entropy source for the proposed TRNG, and the changing input voltage and
 125 the random interval sampling resemble a chaotic map, which further accelerates the changing
 126 process of the input signal, making D_{ADC} with extremely high randomness.

127 The main innovation of this paper lies in the proposition of a mechanism with the
 128 combination of variable analog input signals and ADC random interval sampling, which is
 129 very suitable for low-power application scenarios, especially with WSN nodes. Wireless
 130 sensor network nodes need ADC to collect data, and directly use the sensor circuit as the
 131 entropy source circuit of TRNG, which do not need to add any additional circuit. This results
 132 in an enormous reduction on the system design and manufacturing costs, as well as the power
 133 consumption.

134 The rest of this paper is arranged as follows. Section II analyzes chaotic systems. Section III
 135 elaborates in detail the mathematical model and implementation method of TRNG based on
 136 ADC. Section IV introduces the simulation and verification of the proposed mathematical
 137 model. Section V proposed TRNG implementation and verification. Section VI concludes the
 138 paper with the value and the prospect of the work.

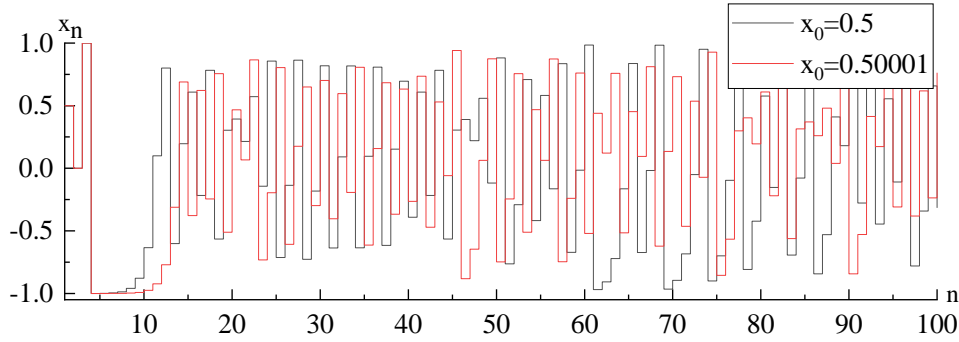
139 **Random Analysis of Chaotic Map**

140 In the chaotic map system, even if the initial conditions are slightly different, the system can
 141 produce completely different output results after multiple iterations [45]. Among the methods
 142 to implement chaotic map, the most widely used is the chaotic map based on 1-D linear
 143 piecewise affine Markov (PWAM) [34,46,47]. To achieve a 1-D linear PWAM map, the
 144 conditions in equation (1) must be satisfied [34].

$$145 \quad X_n = f(X_{n-1}), \quad n = 0, 1, 2, 3, \dots \quad (1)$$

146 Where n is the number of time steps (number of iterations), X_0 is the initial state of the
 147 system, and X_n is the state of the system after n steps of iteration. and the domain of $f(x)$ is the
 148 same as its range. A typical example to further explain how PWAM works can be illustrated
 149 as follows, where $f(x)$ is defined as in equation (2):

$$150 \quad f(x) = \begin{cases} 3x + 2.00001, & \text{if } -1 \leq x < -1/2 \\ x + 1, & \text{if } -1/2 \leq x < 0 \\ -2x + 1.00001, & \text{if } 0 \leq x \leq 1 \end{cases} \quad (2)$$



151

152

Fig. 2 sensitivity of chaotic maps to initial values

153 The definition domain of $f(x)$ is within $[-1,1]$, and 0.00001 in the map can avoid the situation
 154 where the simulation data is always equal to the boundary value (similar to overflow of an
 155 actual circuit. It will lead to the degradation of the random quality of the system. Therefore,
 156 special treatment is needed to avoid the overflow.). In the process of research, two slightly
 157 different initial values are used to observe how the output X_n of the PWAM map varies with
 158 the number of iterations. The first operated initial value X_0 is 0.5 , and the second $X_0=0.50001$.
 159 The difference between the two initial values is 0.00001 , and the number of iterations of each
 160 run is $n=100$. The results of the two runs are shown in Fig. 2 above.

161 As can be seen, after 7 iterations, X_n starts to show obvious differences, and the differences
 162 become increasingly big, as the number of iterations increases. This is sufficient to indicate
 163 that even without noise, due to the limited precision of the system, long time of iterations
 164 entails the unpredictable characteristics of PWAM chaotic map, which is exactly what RNs
 165 featured by. Specifically, there are three essential criteria for RNs [48]:

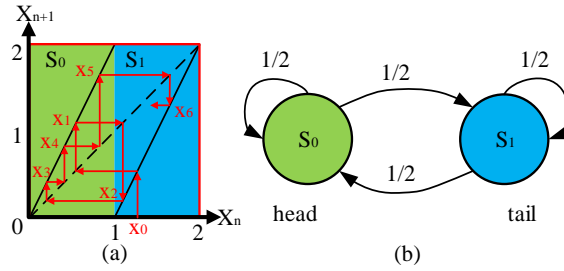
- 166 1. It looks random and can pass the random statistical tests.
- 167 2. It is unrepeatable. Its next bit is an uncertainty between being 0 or 1, even if the algorithm
 168 that produces the sequence and any already produced number of sequences are known.
- 169 3. It is unrepeatable. The obtained sequence is diverse, even with entirely identical input,
 170 under the circumstance of the same algorithm and hardware circuit.

171 Compared with PRNs which only require the first of the above criterions to be satisfied,
 172 TRNs demand all the listed three criterions to be simultaneously satisfied. Briefly speaking,
 173 the next symbol of a random number must be independent of the previously generated
 174 symbol, which is similar to a Markov process. This further illustrates that random number
 175 generators can be implemented by 1-D linear PWAM chaotic map. In terms of PWAM
 176 chaotic maps, Bernoulli shift map is one of the most extensively used one. It can be
 177 represented by equation (3), whose definition domain ranges between $[0,2]$. When $N_{noise}=0$,
 178 its corresponding map is shown in Fig. 3 (a). When the initial value x_0 is different, varied
 179 output sequences will be generated. In addition, the system has only two states: S_0 and S_1 ,
 180 state jump probability is 0.5 , resembling the fair coin toss, as demonstrated in Fig. 3 (b),
 181 which corresponds to a true random system [35].

182

$$f(x_n) = \begin{cases} 2x_n + N_{noise}, & \text{if } 0 \leq x_n < 1 \\ 2x_n - 2 + N_{noise}, & \text{if } 1 \leq x_n \leq 2 \end{cases} \quad (3)$$

183



184

185

Fig. 3 Linear Markov map.
 (a) corresponding linear Markov map, (b) Markov chain of the toss of an unbiased coin.

186
 187
 188
 189
 190
 191
 192
 193
 194

What must be noted is that TRNs cannot be achieved using PWAM alone, because PWAM is a deterministic system. In response, an unpredictable initial state for PWAM shall be provided. In real circuits, a common approach to provide the entropy source information for PWAM is to add some analog devices, such as diodes and transistors. The behavior of these analog devices might bring some minor changes under the influence of noise. It happens because PWAM is very sensitive to small inputs. Therefore, the combination of these analog devices and PWAM empowers the system to generate truly unpredictable behaviors, thus achieving TRNG. In equation (3), PWAM based on Bernoulli shift map can be employed to implement TRNG, When N_{noise} is not zero and the noise comes from the circuit.

195
 196
 197
 198
 199
 200
 201
 202
 203
 204
 205
 206
 207

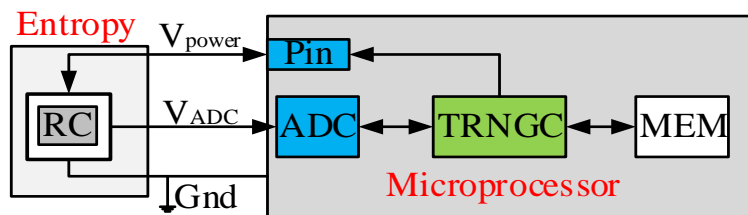
In the 1-D linear PWAM described above, its constraint range (domain) is $[-1,1]$ and $[0,2]$. But in actual circuits, the output can easily exceed the constraint range, because of the influence of noises, which makes it difficult for the chaotic map to return to the normal map range, resulting in the degradation of the randomness quality of the system [49]. However, providing sufficient redundancy for the system state can effectively remove the constraint problem. A prevalent method is to implement Bernoulli shift map to eliminate the constraint problem by ADC [1,2,25,26,33-35,37-39]. However, previously described methods require special integrated circuits [1,2,26,33-35,37], the addition of complex circuit structures to microprocessors [38,39], or the input of noise with statistical characteristics [25]. All these methods would bring great limitations to the application of TRNG. Fortunately, to overcome the above challenges, this paper proposes a common circuit architecture of simple structure and low-cost, which can be implemented either on a custom chip or on a traditional microprocessor (with embedded ADC).

208 The Structure of Proposed TRNG

209
 210
 211
 212

The architecture of the proposed TRNG based on ADC nonlinear effect and chaotic map is shown in Fig. 4. It consists an entropy source circuit and a microprocessor, where the microprocessor includes an ADC, a Memory, a True Random Number Generator Control (TRNGC) module, and configurable pins.

213



214

Fig. 4 The proposed true number generator based on ADC

215 The core of the entropy source circuit is an RC circuit (any other circuits with the same
 216 function of RC circuit can also be used), which is used to realize a changeable voltage signal.
 217 V_{power} is controlled by TRNGC, and when V_{power} is high (V_{cc}), the RC circuit realizes
 218 charging function; when V_{power} is low (Gnd), the RC circuit realizes discharging function.
 219 Therefore, by controlling V_{power} , TRNGC controls the RC circuit to produce a constantly
 220 changing output voltage. ADC is also controlled by TRNGC in order to sample the produced
 221 changing output voltage signal, and because the sampling interval is random, the digital data
 222 has strong randomness. The biggest advantage of this architecture is that it can be used as a
 223 TRNG and a sensor information collecting (the entropy source circuit seen as the sensor
 224 circuit). As a result, when this method is used in sensor equipment of IoT, it is not necessary
 225 to add any hardware circuits, because the sensor equipment normally have general-purpose
 226 devices such as ADCs and sensors. Therefore, the TRNG proposed in this paper has strong
 227 compatibility and can be used in traditional circuit structures.

228 A) TRNG Working Principle

229 For a single-stage ADC with N-bit rounding-down, when the input signal is within the ideal
 230 conversion range, the output is:

$$231 \quad D_{ADC} = ADC(V) = \left\lfloor \frac{2^N}{V_{cc}} V_{ADC} \right\rfloor \quad (4)$$

232 where D_{ADC} represents the digital output signal after ADC conversion, $ADC(\bullet)$ represents
 233 ADC conversion function, $\lfloor \bullet \rfloor$ represents rounding-down operation, V_{CC} represents the
 234 reference voltage of ADC, and V_{ADC} represents the input voltage of ADC. (4) is the working
 235 principle of traditional ADC, and in this paper, the proposed TRNG implemented is based on
 236 traditional ADC, RC circuit and random interval sampling mechanism. The following
 237 equation is used to express the map between the input and output of the entire system:

$$238 \quad x_{n+1} = M(x_n) \quad (5)$$

239 where $M(\bullet)$ represents the map function of the proposed system, x_n represents the input
 240 signal, and x_{n+1} represents the output signal of the map. Next, the expression of the map
 241 function of the proposed TRNG will be derived and discussed.

242 In Fig. 4, assuming that when V_{power} is high or low, the entropy source circuit realizes a
 243 simple RC charging or discharging function, then the output voltage can be calculated as
 244 follows:

$$245 \quad V_{ADC} = \begin{cases} V_0 + (V_{power} - V_0) * (1 - e^{-t/RC}) + V_{noise} & \text{(Charge)} \\ V_0 * e^{-t/RC} + V_{noise} & \text{(Discharge)} \end{cases} \quad (6)$$

246 where V_{ADC} represents the output voltage of the entropy source circuit, which is also the input
 247 voltage of ADC, V_{power} represents the output voltage of MCU pin, RC represents the product
 248 of the equivalent resistance and equivalent capacitance of the entropy source circuit, and
 249 V_{noise} represents the noise of the circuit. When $t = 0$, $V_{ADC} = V_{power} + V_{noise}$, thus V_{ADC} only
 250 changes with noise. When $t \geq 5RC$, V_{ADC} output is stable, and if it is a charging process, V_{ADC}
 251 $= V_{power} + V_{noise}$; if it is a discharging process, $V_{ADC} = V_{noise}$. The entropy source circuit can be

252 treated as a resistor divider circuit when $t = 0$ or $t \geq 5RC$ (resistance is infinitely large and
 253 infinitely small). However, the entropy source information of the system input is only
 254 decided by noise [25], causing weak randomness (the traditional low precision ADC is hard
 255 to identify noises). Therefore, in order to improve the randomness, it is necessary to ensure
 256 that during the ADC sampling process, the charge and discharge state must be switched for
 257 every $5RC$ duration. Another problem is that the value of RC changes in the actual circuit,
 258 thus the charging and discharging time cannot be accurately controlled. Therefore, in order to
 259 prevent V_{ADC} from remaining a stable state, two thresholds are set: a high threshold (D_{HT}) and
 260 a low threshold (D_{LT}). When V_{ADC} surpasses D_{HT} , the RC circuit begins to discharge, and
 261 when V_{ADC} reaches below D_{LT} , the RC circuit begins to charge. The following equation can
 262 be used to express the state of the system after a long-time operation:

$$263 \quad V_{ADC}^{k+1} = \begin{cases} V_{ADC}^k + (V_{ADC}^{power} - V_{ADC}^k) * (1 - e^{-t/RC}) + V_{ADC}^{noise} & \text{(Charge)} \\ V_{ADC}^k * e^{-t/RC} + V_{ADC}^{noise} & \text{(Discharge)} \end{cases} \quad (7)$$

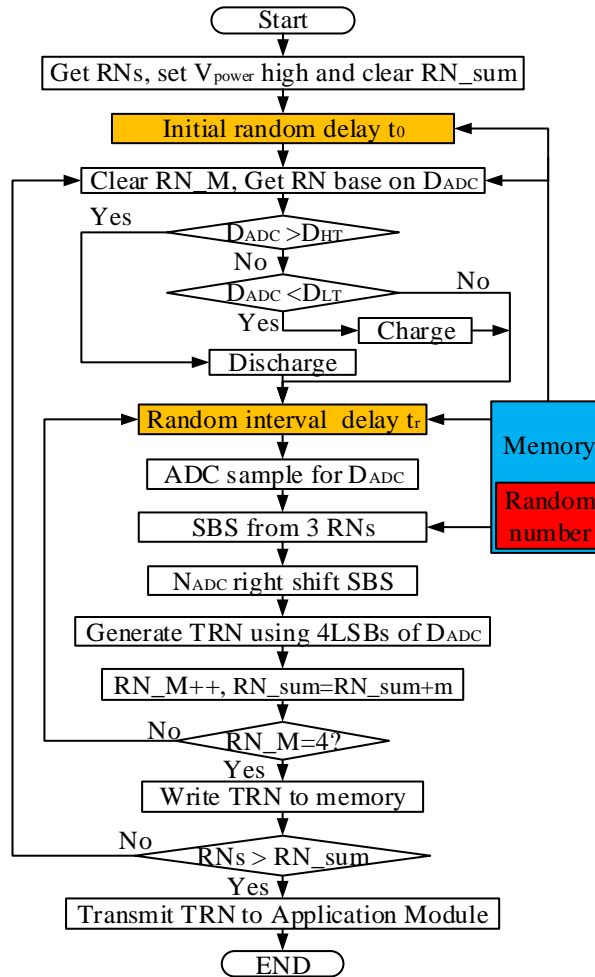
264 where k represents the number of sampling times. From (7), it can be seen that V_{ADC}^{k+1} is
 265 affected by noise, as well as k and t . In other words, after the RC circuit starts charging or
 266 discharging, even if initial V_{ADC} is unchanged (noise is ignored), the randomness of V_{ADC}^{k+1} can
 267 be improved through TRNG by controlling the value of V_{power} and ADC sampling interval
 268 (time t). Additionally, with the increase of the number of iteration times k , a completely
 269 different data set V_{ADC}^{k+1} , $k > 0$ can be obtained, making the system to have certain chaotic
 270 map characteristics. The microprocessor then converts V_{ADC}^{k+1} into a digital
 271 signal D_{ADC}^{k+1} through ADC, and generates TRNs with high randomness using each
 272 converted D_{ADC}^{k+1} . Furthermore, in (7), the randomness of the system can be further improved
 273 by controlling the charge and discharge conditions (charge and discharge threshold).

274 **B) TRNG Implementation**

275 In order to improve the performance of the proposed TRNG to generate TRNs, random
 276 numbers are used to generate threshold voltages D_{HT} and D_{LT} . Moreover, a cyclic shift is
 277 performed on D_{ADC}^{k+1} , and the lower 4-bits of the shifted data is used to generate TRNGs, which
 278 effectively improves the production efficiency of TRNG. The steps of implementation of the
 279 proposed TRNG to generate TRNs are as follows:

- 280 1, Firstly RNs , representing the number of digits of the random numbers to be generated, is
 281 determined, V_{power} is set to high, and RN_sum is cleared. Then TRN_0 , representing the last
 282 stored true random number, is extracted from a specific address to generate an initial
 283 random delay t_0 based on (9).
- 284 2, After the initial random delay, D_{ADC}^k (firstly 0) is compared with D_{HT} and D_{LT} . When it is
 285 greater than D_{HT} , set V_{power} to 0 and the entropy source circuit starts to discharge; when it
 286 is less than D_{LT} , set V_{power} to 1 and the entropy source circuit starts to charge.
- 287 3, Next, the true random number TRN_{DADC} , is extracted from memory using the lower 8 bits
 288 of D_{ADC}^k as the relative address. Then using TRN_{DADC} , a random interval delay t_r is
 289 generated based on (10).
- 290 4, After the random interval delay, V_{ADC} signal is sampled using ADC to obtain digital data
 291 D_{ADC}^{k+1} . Based on D_{ADC}^{k+1} , three generated TRNs are extracted from the memory, whose LSBs

- 292 are then used to form a 3-bit data, represented as SBS. Then, an SBS-bit cyclic shift is
 293 performed on D_{ADC}^{k+1} to obtain D_{ADC}^{SBS} , and the last 4 bits is extracted to generate the TRNs
- 294 5, Step (3) and (4) 4 are repeated four times to obtain a 16-bit TRN before it is written to
 295 memory. The address of TRN is automatically added by 1, and copied to a specific address.
- 296 6, Finally, whether to continue generating a new map is determined. If yes, skip to step 2;
 297 otherwise, the generated TRN is sent to the application module.



298

299

Fig. 5. Flow chart for generating map

300 The detailed workflow of the proposed TRNG is shown in Fig.5, where RN_M is the number
 301 of cyclic sampling (here set to 4), and RN is the TRN from memory, used to generate D_{HT} and
 302 D_{LT} , which enables a changeable threshold function, resulting in effectively improved
 303 randomness of TRN.

304 C) Proposed TRNG Performance Analysis

305 In Fig. 5, the unit time of the initial random delay and random interval delay is the clock
 306 cycle of the microprocessor, and the initial random delay t_0 is determined by the last
 307 generated TRN. The initial random delay follows the equation:

308
$$t_0 = \frac{1}{f_P} TRN_0 \& \text{const1} \quad (8)$$

309 where f_P represents the frequency of the microprocessor, $\&$ represents the bitwise AND, and
 310 const1 represents a constant number. For example, $\text{const1}=15$ (indicates F in hexadecimal
 311 notation). Therefore, $TRN_0 \& \text{const1}$ represents the extraction of the last four digits of TRN_0 .

312 Similarly, the random interval delay follows the equation:

313
$$t_r = \frac{1}{f_P} TRN_{D_{ADC}} \& \text{const2} \quad (9)$$

314 where D_{ADC} represents the output signal after ADC sampling, whose lowest 8 bits are used as
 315 the relative address to extract the TRN of the corresponding address in the memory (indicated
 316 by $TRN_{D_{ADC}}$), const2 represents a constant, similar to const1 .

317 Before and after ADC sampling, the microprocessor needs a certain amount of time t_p to
 318 process data (determined by the working frequency and the number of clock cycles).
 319 Assuming that the microprocessor takes cnt clock cycles in total to process data, then:

320
$$t_p = \frac{\text{cnt}}{f_P} \quad (10)$$

321 Therefore, according to (5) ~ (11), and take $k=0$ into consideration, the equation of V_{ADC}^{k+1} with
 322 ADC sampling times can be obtained as follows:

323
$$V_{ADC}^{k+1} = M(V_{ADC}^k) = \begin{cases} V_{ADC}^{power} \left(1 - e^{-\sum_{i=0}^k ((t_0+t_r+t_p)/(RC))}\right) + V_{ADC}^{noise}, & \text{if (*1)} \\ V_{ADC}^{kl} + (V_{ADC}^{power} - V_{ADC}^{kl}) \left(1 - e^{-\sum_{i=k+1}^k ((t_0+t_r+t_p)/(RC))}\right) + V_{ADC}^{noise}, & \text{if (*2)} \\ V_{ADC}^{kh} * e^{-\sum_{i=k+1}^k ((t_0+t_r+t_p)/(RC))} + V_{ADC}^{noise}, & \text{if (*3)} \end{cases} \quad (11)$$

324 where t_s represents the time consumed by ADC to achieve digital-to-analog conversion, (*1)
 325 represents $k=0$, (*2) represents $D_{ADC}^{kl} < D_{LT} \& D_{ADC}^k < D_{HT}$, and (*3) represents $D_{ADC}^{kh} >$
 326 $D_{HT} \& D_{ADC}^k > D_{LT}$. V_{ADC}^{kl} and V_{ADC}^{kh} represents the input voltage value of ADC when
 327 $D_{ADC}^{kl} < D_{LT}$ and $D_{ADC}^{kh} > D_{HT}$, respectively. (11) shows the map relationship between V_{ADC}^{k+1}
 328 and V_{ADC}^k (D_{ADC}^{k+1} and D_{ADC}^k in the microprocessor), which is similar to 1-D linear piecewise
 329 affine Markov. Noise V_{noise} directly affects D_{ADC}^{k+1} , and the randomness of D_{ADC}^{k+1} is further
 330 improved by V_{noise} through the parameters t_0 , t_r , V_{LT} and V_{HT} . Furthermore, from the character
 331 of ADC and (4), it can be derived that DADC, the output signal of ADC, has certain non-
 332 linear characteristics and quantization errors, which will also increase the randomness of
 333 D_{ADC}^{k+1} . Therefore, using the map in (11) to implement TRNG has more randomness than using
 334 the periodic sampling level fixed in ADC [25] (only noise changes).

335 According to (11), the time required for ADC to sample k times is:

336
$$t = t_0 + k * (t_r + t_p + t_s) \quad (12)$$

337 Take TMS320F2803x, a microprocessor on the market, for example, its sampling frequency
 338 can reach 3 MHz, and its main frequency can reach $fp=60$ MHz (other microprocessors, such
 339 as DSP and ARM, etc., have higher sampling frequencies and main frequencies that can
 340 further improve the efficiency of TRNG to generate map). The processing consumes about 60
 341 clock cycles, and after testing, when $const1=const2=63$, the randomness basically meets the
 342 requirements. When the lowest 6 bits of TRN_0 and TRN_{DADC} are both 1, the time consumed is
 343 the longest, which takes 16 clock cycle. Then the time can be calculated as:

344
$$t = \frac{63}{fp} + k * \left(\frac{63}{fp} + \frac{60}{fp} + \frac{1}{fs} \right) = \frac{63}{60} + k * \left(\frac{63}{60} + 1 + \frac{1}{3} \right) \quad (13)$$

345 When $k=1$, the result is 3.43 us, which is 0.29 Mbps. i.e. the slowest rate of generating map is
 346 0.29 Mbps. Similarly, the average rate of generating map is calculated to be 0.42 Mbps (TRN_0
 347 and TRN_{DADC} both take half of their maximum value). Everytime a 4-bit true random number
 348 is generated for each sampling (Table 2 verifies its feasibility), it can be obtained that the
 349 proposed TRNG generates a true random number at a rate of about 1.68 Mbps.

350 **Simulation and Verification**

351 The sources of randomness of the proposed TRNG in this paper mainly include: 1) circuit
 352 noise, 2) ADC nonlinearity, 3) random interval sampling, 4) varying input voltage (noise not
 353 included). Among them, circuit noise and ADC nonlinearity add uncertainty to the system,
 354 while random interval sampling and varying input voltage provide the system with the
 355 characteristics of chaotic map. The combination of the two can achieve high-performance
 356 TRNG. Since the ADC nonlinearity is an inherent characteristic of the chip (during
 357 simulation, only the quantization error of ADC is considered), we mainly simulate the
 358 performance of the proposed chaotic map and the performance of TRNG based on the map.

359 **A) Performance Analysis of the varied input and random intervals**

360 To simplify the analysis, a linear input signal with the slope of 1 is used to replace the RC
 361 circuit, and four different situations are simulated in order to analyze the performance of the
 362 proposed chaotic map. On the one hand, the four situations are divided into two by the input
 363 signal of ADC:

- 364 (1) A 1V constant voltage superimposed with a 1 mV average noise,
 365 (2) A linearly rising voltage with slope is 1 superimposed with a 1mV average noise.

366 On the other hand, the four situations are divided into two by the sampling frequency:

- 367 (1) ADC performs periodic sampling,
 368 (2) ADC performs sampling at random intervals.

369 In other words, the 4 simulation situations are: (1) $V_{ADC}=1+\text{noise}$ (without random intervals),
 370 (2) $V_{ADC}=1+\text{noise}$ (with random intervals), (3) $V_{ADC}=t+\text{noise}$ (without random intervals), (4)

371 $V_{ADC} = t + \text{noise}$ (with random intervals). The lowest bit of D_{ADC} is used to generate random
372 numbers, and $4 \times (10^6)$ bits of data is produced for each simulation situation. Finally, the
373 randomness of the generated random numbers is verified using the U.S. National Institute of
374 Standards and Technology (NIST) [50] test suite, and the results are shown in Table 1 ($p \geq$
375 0.01 indicates that the test is passed, “Pass” indicates that all subcases pass the test and “Fail”
376 is the opposite of pass). It can be seen from the table that when $V_{ADC} = 1 + \text{noise}$, the NIST
377 verification result is very poor regardless of whether random intervals are added between
378 ADC samples. When $V_{ADC} = t + \text{noise}$ and no random interval is added between ADC samples,
379 the NIST verification result is also very poor, but the results are much better than the former
380 situation. Furthermore, when $V_{ADC} = t + \text{noise}$, by adding random intervals between ADC
381 samples, the results verified by NIST indicates the effectiveness of our proposed chaotic map
382 in improving randomness.

383 In (1) and (2), because the input signal is fixed, only the circuit noise changes. However, the
384 noise in the circuit is so small that the accuracy of the 12-bits ADC is not enough to sample
385 the noise directly. As a result, the D_{ADC} sampled by ADC is almost fixed. In (3), because the
386 input is changing, the nonlinear effect of ADC can result in a certain degree of randomness in
387 D_{ADC} . From the results, it can be seen that the randomness in (3) is better than that in (1) and
388 (2). However, because the input voltage is linearly changing in (3), it is difficult to drastic
389 change the time interval of ADC sampling just relying on noise and nonlinear characteristics
390 of ADC. Consequently, that the interval of each ADC sampling does not change much,
391 resulting in low randomness of D_{ADC} . In (4), random interval is added, which can further
392 influence the sampling interval based on D_{ADC} , so that the data of each sampled D_{ADC} is
393 completely different, and true random numbers can be generated.

394

Table 1: True random number simulation verification results

| NIST- sts-2.1.2, randomness test | $V_{ADC} = 1 + \text{noise}$ (without random interval) | | $V_{ADC} = 1 + \text{noise}$ (with random interval) | | $V_{ADC} = t + \text{noise}$ (without random interval) | | $V_{ADC} = t + \text{noise}$ (with random interval) | | Proposed TRNG | |
|-------------------------------------|--|-------|---|-------|--|---------|--|---------|---------------|---------|
| | P-value | Prop. | P-value | Prop. | P-value | P-value | Prop. | P-value | Prop. | P-value |
| Frequency | <0.01 | 0/10 | <0.01 | 0/10 | <0.01 | 6/10 | 0.21331 | 10/10 | 0.534146 | 10/10 |
| Block Frequency | <0.01 | 5/10 | <0.01 | 3/10 | 0.350485 | 10/10 | 0.739918 | 10/10 | 0.122325 | 10/10 |
| Cumulative Sums 0 | <0.01 | 0/10 | <0.01 | 0/10 | <0.01 | 6/10 | 0.739918 | 10/10 | 0.122325 | 10/10 |
| Cumulative Sums 1 | <0.01 | 0/10 | <0.01 | 0/10 | <0.01 | 6/10 | 0.911413 | 10/10 | 0.534146 | 9/10 |
| Runs | <0.01 | 0/10 | <0.01 | 0/10 | 0.213309 | 10/10 | 0.534146 | 10/10 | 0.911413 | 10/10 |
| Longest Run | <0.01 | 0/10 | <0.01 | 0/10 | 0.739918 | 10/10 | 0.350485 | 10/10 | 0.534146 | 10/10 |
| Rank | 0.350485 | 10/10 | 0.911413 | 10/10 | 0.534146 | 10/10 | 0.739918 | 10/10 | 0.739918 | 9/10 |
| FFT | 0.350485 | 10/10 | 0.122325 | 10/10 | 0.739918 | 10/10 | 0.911413 | 10/10 | 0.213309 | 10/10 |
| Non Overlapping Template | Fail | Fail | Fail | Fail | Fail | Pass | Pass | Pass | Pass | Pass |
| Over lapping Template | <0.01 | 3/10 | <0.01 | 4/10 | 0.739918 | 10/10 | 0.739918 | 10/10 | 0.534146 | 10/10 |
| Universal | 0.350485 | 10/10 | 0.739918 | 10/10 | 0.122325 | 10/10 | 0.350485 | 10/10 | 0.017912 | 10/10 |
| Approximate Entropy | <0.01 | 0/10 | <0.01 | 0/10 | 0.350485 | 10/10 | 0.739918 | 10/10 | 0.534146 | 10/10 |
| Random Excursions | Fail | Fail | Fail | Fail | - | Pass | - | Pass | - | Pass |
| Random Excursions Variant | Fail | Fail | Fail | Fail | - | Pass | - | Pass | - | Pass |
| Serial 0 | 0.122325 | 8/10 | 0.213309 | 8/10 | 0.534146 | 10/10 | 0.911413 | 10/10 | 0.534146 | 10/10 |
| Serial 1 | 0.122325 | 10/10 | 0.350485 | 10/10 | 0.350485 | 9/10 | 0.066882 | 10/10 | 0.911413 | 10/10 |
| Linear Complexity | 0.350485 | 10/10 | 0.017912 | 10/10 | 0.213309 | 10/10 | 0.213309 | 10/10 | 0.017912 | 10/10 |

395 B) Performance Analysis of the Proposed TRNG

396 In the previous section, we have verified that the proposed chaotic map can effectively
397 improve the system's performance in generating random numbers. However, only the LSB
398 output from ADC is used to generate random numbers (1 bit of random number is extracted

399 after each ADC sampling), which is less efficient. In this section, the entropy source circuit
 400 of the proposed TRNG can use an RC circuit to obtain more than a simple linear function,
 401 and the randomness of the RC output signal is also improved by controlling it to constantly
 402 charge and discharge. In addition, this paper proposes to use cyclic shift to process D_{ADC}
 403 during post-processing, and the lowest 4 bits of the processed data are used to generate the
 404 true random number, which can improve the efficiency of the TRNG greatly.

405 In traditional data interaction, most of the methods use integer multiples of bytes for data
 406 interaction. In order to achieve generality, integers multiples of 16 bits are generated each time
 407 when true random numbers are generated. Since the lowest 4 bits of D_{ADC} of each ADC
 408 sampling data is used to generate true random numbers, four times of ADC sampling is required
 409 to obtain a true random number of $4*4=16$ bits. The TRNG represented by (11) is simulated
 410 here, and its flow is shown in Fig. 5, where m represents the number of ADC cycles, RNs
 411 means that at least bits true random number is generated each time. In Fig. 5, sets $m=4$ and
 412 RNs=16, and the simulation algorithm is shown in Algorithm 1.

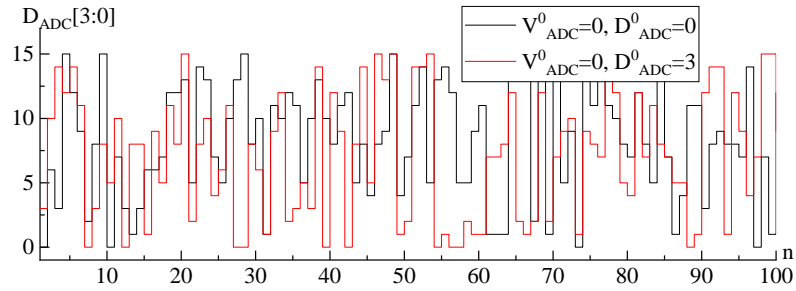
Algorithm 1 TRNG simulation algorithm based on ADC nonlinear effect and chaotic map

Input: m , RNs, const1, const2, SNR= 10^6

Output: TRNs

1. Set V_{power} high, for charging input voltage V_{ADC}
 2. Get TRN_0 and calculate t_0 based on (8)
 3. Dealy_function (t_0)for intial delay
 4. Get RN base on D_{ADC}
 5. Calcuete V_{HT} and V_{LT} base on RN, which compare with D_{ADC} for charge or discharge V_{ADC}
 6. Get TRN_{DADC} base on D_{ADC} , and calculate t_r based on (9)
 7. Dealy_function (t_r) for random delay
 8. ADC samples, $D_{ADC} = \lfloor 2^N V_{in} / V_{cc} \rfloor$
 9. Get three RNs for SBS, and N_{ADC} right shift SBS bits
 10. Extract 4 LSBs from shifted N_{ADC} for generating TRN
 11. **If** RN_M = m **Then**
 Write TRN to memory and Jump to step 12
 Else
 Jump to step 6
 End If
 12. **If** RNs > RN_sum **Then**
 Exit
 Else
 Jump to step 4
 End If
-

413 Under the same initial conditions, which means that the input V_{ADC} of ADC is 0, and the
 414 $D_{ADC}^{0} [3:0]$ obtained from the first sampling of ADC are 0 and 3, respectively. two
 415 simulations are conducted on Algorithm 1, each iterated 100 times. Fig. 6 shows the lowest 4
 416 bits of D_{ADC} . It can be seen from the figure that the output data of the two simulations are
 417 different, which implies that the proposed TRNG architecture has non-repeatable
 418 characteristics. i.e. even if the initial conditions are the same, D_{ADC} will be completely
 419 different due to circuit noise and ADC nonlinear characteristics. Furthermore, the simulation
 420 generated a $4*(10^6)$ bits random number and the random numbers are verified using NIST.
 421 The verification results are shown in the “proposed TRNG” column in Table 1, which
 422 suggests that the proposed TRNG has good performance on the randomness of its output.



423

424

Fig. 6 Comparison of $D_{ADC} [3:0]$ between two simulations

425 It can be seen from the simulation results of sec. IV-A and sec. IV-B, that the changing input
 426 voltage and random interval sampling have the characteristics of chaotic map. Moreover,
 427 combining them with circuit noise and ADC nonlinearity can achieve high-performance and
 428 high-efficiency TRNG.

429 Implementation and Validation

430 The structure of the proposed TRNG in this paper is very simple and has strong
 431 compatibility. It is especially suitable for sensing equipment, which the sensor circuit can be
 432 directly used as the entropy source circuit without adding any additional circuit. In order to
 433 demonstrate its compatibility and advantages in the field of WSN for the IoT, we
 434 implemented two proposed TRNG based on RFID tags of separated components:

435 1) The entropy source circuit adopts a pure RC circuit, which is a general structure for
 436 proposed TRNG. RC can be adjusted freely to improve the performance of the proposed, and
 437 its structure is shown in Fig. 7 (a).

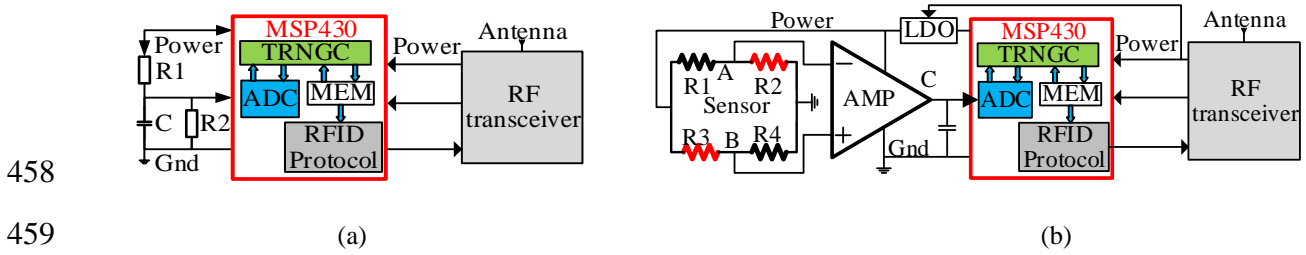
438 2) The entropy source circuit adopts sensor circuit, which is a special structure by proposed
 439 TRNG and is mainly used in sensing devices of the IoT. No additional circuit is needed,
 440 which greatly reduces the cost of TRNG, and its structure is shown in Fig. 7 (b).

441 The TRNG whose entropy source is based on RC circuit, is specially used to generate true
 442 random numbers (no other functions). The value of RC can be arbitrarily adjusted in order to
 443 get TRNG with good performance. The TRNG based on sensing circuit as entropy source is
 444 generally used in scenarios compatible with sensor functions. In such case, the sensor circuit
 445 is mainly used for sensing functions, while the TRNG is an incidental function, which can
 446 generate true random numbers without occupying any hardware resources, and with lower
 447 cost and simpler design.

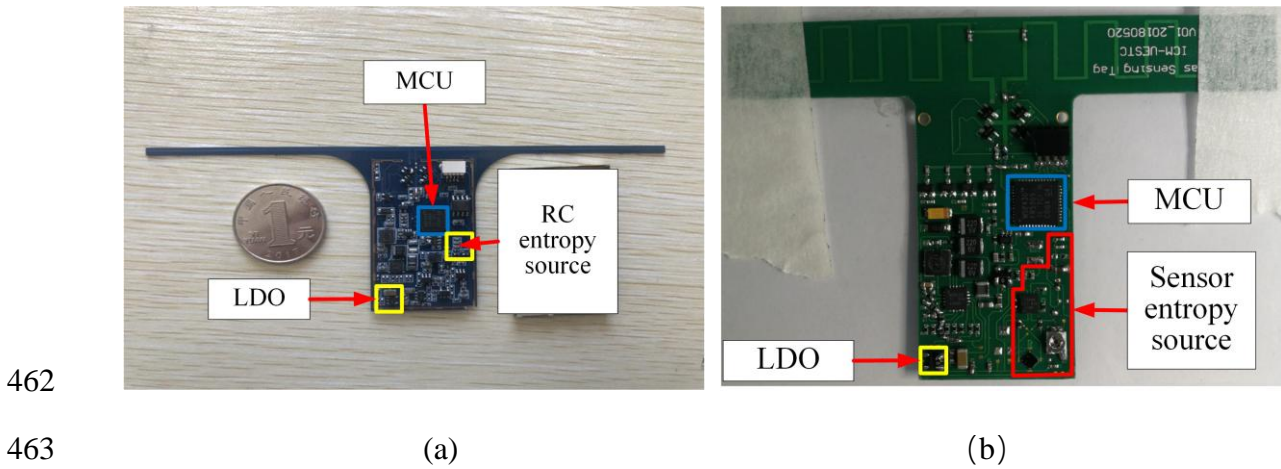
448 In this paper, the microprocessor MSP430 (embedded 12-bits ADC) [51] is used to
 449 implement the RFID Protocol and realize the software control of the TRNG. LDO provides a
 450 stable voltage to the sensor circuit, AMP is used to amplify the output signal of the sensor,
 451 TRNGC is the control module, and MEM is the built-in memory of the MSP430.

452 The hardware object of the proposed TRNG is shown in Fig. 8, Fig. 8 (a) and Fig. 8 (b) show
 453 the general RC structure and the sensor circuit for entropy source circuit, respectively. Here
 454 the Fig. 8 (b) is a special structure of proposed TRNG, which can not only realize TRNG, but
 455 also can realize the function of information sensing. Moreover, the true random number can

456 be used to increase the reliability of the encryption algorithm, so as to further improve the
 457 communication security of wireless sensor network.



460 Fig. 7. The structure of proposed TRNG, (a) The general structure of proposed TRNG, (b) A special general
 461 structure of proposed TRNG



464 Fig. 8. The TRNG is based on RFID sensor tag. (a) Entropy source is RC circuit, (b) Entropy source is sensor
 465 circuit

466 Table 2: True random number test results

| NIST- sts-2.1.2, randomness test | Proposed TRNG (sensor circuit) | | | | | | | | Proposed TRNG (RC) | |
|-------------------------------------|--------------------------------|-------|---------------------|-------|---------------------|---------|---------------------|---------|--|---------------------|
| | 1 st LSB | | 2 nd LSB | | 3 rd LSB | | 4 th LSB | | 1 st ~4 th -LSBs | 1 st LSB |
| | P-value | Prop. | P-value | Prop. | P-value | P-value | Prop. | P-value | Prop. | P-value |
| Frequency | 0.739918 | 1 | 0.964295 | 1 | 0.637119 | 1 | 0.534146 | 1 | 0.637119 | 1 |
| Block Frequency | 0.122325 | 0.8 | 0.739918 | 1 | 0.534146 | 1 | 0.911413 | 1 | 0.162606 | 1 |
| Cumulative Sums 0 | 0.122325 | 1 | 0.739918 | 1 | 0.437274 | 1 | 0.534146 | 1 | 0.911413 | 1 |
| Cumulative Sums 1 | 0.534146 | 0.9 | 0.437274 | 1 | 0.534146 | 1 | 0.739918 | 1 | 0.213309 | 1 |
| Runs | 0.534146 | 0.9 | 0.275709 | 1 | 0.437274 | 1 | 0.213309 | 1 | 0.017912 | 0.95 |
| Longest Run | 0.350485 | 1 | 0.637119 | 0.95 | 0.964295 | 1 | 0.350485 | 1 | 0.834308 | 1 |
| Rank | 0.534146 | 1 | 0.834308 | 1 | 0.911413 | 0.9 | 0.122325 | 1 | 0.964295 | 1 |
| FFT | 0.534146 | 1 | 0.739918 | 1 | 0.534146 | 1 | 0.739918 | 1 | 0.025193 | 1 |
| Non Overlapping Template | Pass | Pass | Pass | Pass | Pass | Pass | Pass | Pass | Pass | Pass |
| Over lapping Template | 0.350485 | 1 | 0.834308 | 1 | 0.350485 | 0.9 | 0.739918 | 1 | 0.534146 | 1 |
| Universal | 0.911413 | 0.9 | 0.213309 | 1 | 0.834308 | 1 | 0.350485 | 1 | 0.035174 | 0.95 |
| Approximate Entropy | 0.122325 | 1 | 0.122325 | 1 | 0.437274 | 1 | <0.01 | 0.9 | 0.035174 | 0.9 |
| Random Excursions | - | Pass | - | Pass | - | Pass | - | Pass | Pass | Pass |
| Random Excursions Variant | - | Pass | - | Pass | - | Pass | - | Pass | Pass | Pass |
| Serial 0 | 0.534146 | 1 | 0.637119 | 1 | 0.162606 | 1 | 0.739918 | 1 | 0.048716 | 1 |
| Serial 1 | 0.534146 | 1 | 0.090936 | 0.95 | 0.739918 | 1 | 0.350485 | 1 | 0.275709 | 1 |
| Linear Complexity | 0.066882 | 1 | 0.437274 | 1 | 0.213309 | 1 | 0.350485 | 1 | 0.739918 | 1 |

467 For TRNG based on sensor circuit, because the adjustable range of sensor circuit is small in
 468 order to realize sensing function, so we use 1-bit of each ADC sample to realize the TRN,
 469 such as the 1st LSB, 2nd LSB, 3rd LSB and 4th LSB of ADC output. In each case, random
 470 numbers of $4 \times (10^6)$ bits are generated. The NIST verification results are shown in the
 471 column of Proposed TRNG (sensor circuit) in Table 2. It can be seen from the test results that
 472 the random numbers generated by the four situations have strong randomness. The
 473 verification results of the Approximate Entropy of the random number generated by 4th
 474 LSB is not good, which can also indicate that the randomness of the generated random
 475 number begins to weaken from the fourth bit of the ADC output. At the same time, we also
 476 implemented TRNG based on RC structure, and adopted the proposed TRNGC process in III-
 477 B. The ADC sampled once to generate 4bits of true random numbers (which is more efficient
 478 than the sensor structure), and a total of $3 \times (10^7)$ bits of random numbers were generated.
 479 The results of NIST is shown in the column of Proposed TRNG (RC) in Table 2. It can be
 480 seen from the results that the Proposed TRNG meets the all requirements of NIST test,
 481 indicating that the Proposed method can be used to realize TRNG.

482 Table 3 lists the performance comparison of a variety of TRNGs, as well as their
 483 compatibility in mainstream microprocessors such as MCU, DSP, ARM, and FPGA, etc. It
 484 can be seen from the table that the proposed TRNG in this paper occupies the least resources,
 485 has low power consumption, and is very compatible. i.e. it can be implemented in various
 486 processors or through simple dedicated chips. The proposed TRNG has great advantages in
 487 low power consumption, low cost, miniaturization, and strictly time required application
 488 scenarios. Moreover, it is particularly suitable to be used in wireless sensor network sensor
 489 equipment without occupying additional circuit resources.

490

Table 3: Performance comparison

| Parameter | This work | [25] | [34] | [12] | [43] | [40] | [41] |
|-------------|-----------|------|---------------|---------------------|-----------------|---------|--------|
| Resources | RC | R | Multi ADCs | 836 μm^2 | 141~2387 LUT-FF | 300 ROs | 5 CLBs |
| Power level | mA | mA | μA | μA | A | A | A |
| MCU | Yes | Yes | No | No | No | No | No |
| DSP | Yes | Yes | No | No | No | No | No |
| ARM | Yes | Yes | No | No | No | No | No |
| FPGA | Yes | Yes | No | No | Yes | Yes | Yes |
| Chip | Yes | Yes | Yes | Yes | Yes | Yes | Yes |
| NIST test | Pass | N/A | Pass | Pass | Pass | Pass | Pass |

491
492

* RC is resistance and capacitance circuits, R is resistance. LUT-FF is Look Up, RO is ring oscillator, CLB is Configurable logical block.

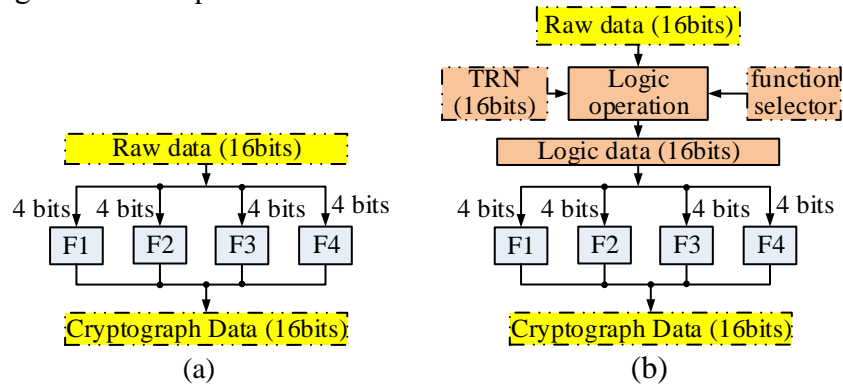
493 From the above equations, simulations, test results and performance comparison, it can be
 494 seen that base on ADC nonlinear chaotic map method proposed in this paper can realize a
 495 TRNG, and compared with other existing TRNG, it has great advantages in terms of low
 496 power consumption, low cost and strong compatibility.

497 Discussion

498 The proposed TRNG in this paper has the characteristics of low power consumption, low
 499 design complexity and strong compatibility, which can be very convenient to be used in the
 500 field of security encryption and anti-collision, especially in the passive sensor tags of the
 501 Internet of things, which has the lowest power consumption.

502 The proposed TRNG is used in secure encryption to improve secure communication
 503 performance of IoT. Taking an encryption algorithm for example, an initial F operation is

504 shown in Fig.9 (a), which the F operation divides the input 16-bit data into four 4bits and
 505 then performing four sub F operations.

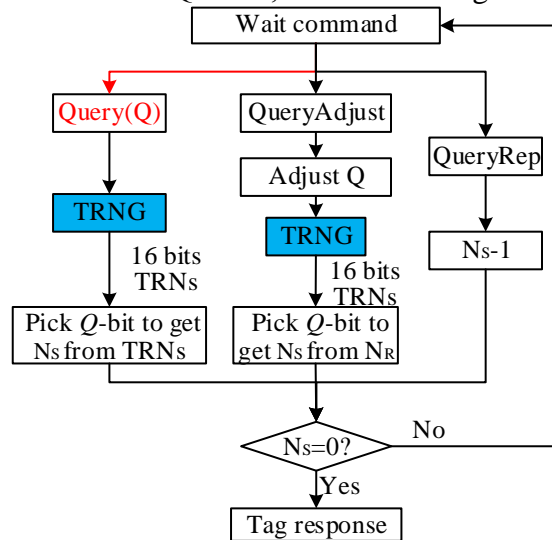


506
 507

508 Fig. 9. F operation structure, (a) original F operation, (b) improved F operation

509 In order to improve the performance of the encryption algorithm, the input data and a 16-bit
 510 TRNs are combined to perform a simple logical operation before F operation, as shown in
 511 Fig.9 (b), where 16-bits TRNs are generated by the proposed TRNG. TRN performs logical
 512 operation with 16-bit raw data to generate logic data, and function selection is used to select
 513 different logical operation operations. For example, if the logical operation is XOR operation,
 514 when $TRN \neq 0$, Logic data is different from raw data, which will result in cryptograph data
 515 being completely different from the original cryptograph data. However, when $TRNs = 0$, the
 516 original data is the same as logic data (raw data XOR 0). Therefore, the improved encryption
 517 algorithm in Fig.9 (b) can not only improve the encryption performance, but also be
 518 compatible with the original encryption algorithm, with huge flexibility.

519 The proposed TRNG can also be used in the anti-collision field of RFID to improve the
 520 efficiency of multi-tag identification. For example, in ISO/IEC 18000-6 Type C Standard
 521 [52], the tag needs to implement pseudo-random number/true random number to implement
 522 the anti-collision algorithm based on Q value, as shown in Fig.10.



523

524 Fig.10. Structure of anti-collision algorithm based on the proposed TRNG

525 The commands related to the anti-collision algorithm include Query, QueryAdjust and
 526 QueryRep. At the beginning of each inventory, the reader needs to send Query command to
 527 determine an initial Q value, and the tag uses the proposed TRNG in this paper to generate a
 528 16-bit random number and intercept the Q-bits generating N_s . Finally, whether to return data
 529 can be determined according to whether the intercepted Q-bits data is 0, and when the
 530 intercepted Q-bits data is not zero, the reader needs to send QueryAdjust and QueryRep

531 commands to control the tag to return the response data. Meanwhile, in the RFID protocol,
532 QueryRep command has the least bits, so its time is the shortest but greater than 25 us. Since
533 the proposed TRNG can generate true random numbers at a rate greater than 1.68Mbps, the
534 proposed TRNG can generate at least 42 bits of true random number in 25 us. Also in RFID
535 protocol, there is a requirement to delay between T1 and T2, which can also be used to
536 generate more TRNs with TRNG. As a result, the process meet the requirement to produce
537 multiple RNGs needed for RFID communication.

538 **Conclusion**

539 This paper introduces the feasibility of using ADC to realize TRNG, and analyzes the
540 shortcomings of existing TRNG based on ADC. A novel TRNG based on ADC nonlinear
541 effect and chaotic map is proposed, which can be realized by using traditional processors
542 with ADC. When the ADC sampling frequency in the processor is 3 MHz and the main
543 frequency is 60 MHz, the proposed TRNG can generate TRNs at a rate of about 1.68 Mbps.
544 The proposed TRNG for sensor tag does not need any additional circuit, which greatly
545 reduces the cost and power consumption of the system. The simulation results show that the
546 proposed structure can effectively improve the randomness of the system. From the test
547 results of the two proposed TRNG, it can be seen that the proposed TRNG not only improves
548 the versatility of the ADC-based TRNG, but also reduces the complexity of the system
549 design, and therefore, it has a very high practical value. In future work, the proposed TRNG
550 in this paper can be integrated into the RFID technology-based sensor tag (chip), which can
551 speed up the construction of communication security in the IoT.

552 **Data Availability**

553 The experimental data used to support the findings of this study are available from the
554 corresponding author upon request.

555 **Conflicts of Interest**

556 The authors of this paper declare that there are no conflicts of interest regarding the
557 publication of this paper.

558 **Acknowledgments**

559 This work was supported in part by the National Key R&D Program under project contract
560 No. 2018YFB1802102 and 2018AAA0103203, in part by the Ministry of Education-China
561 Mobile Fund Program under project contract No. MCM20180104, in part by National
562 Natural Science Foundation of China under project contracts No. 61971113 and 61901095,
563 in part by the Guangdong Provincial Research and Development Plan in Key Areas under
564 project contracts No. 2019B010141001 and 2019B010142001, in part by the Sichuan
565 Provincial Science and Technology Planning Program under project contracts No.
566 2020YFG0039, 2021YFG0013, and 2021YFH0133, in part by the Yibin Science and
567 Technology Program - Key Projects under project contracts no. 2018ZSF001 and
568 2019GY001, in part by the Grant SCITLAB-0010 and SCITLAB-100021 of Intelligent
569 Terminal Key Laboratory of Sichuan Province, and in part by the fundamental research funds
570 for the Central Universities under project contract no. YGX2019Z022. (Corresponding
571 authors: Guangjun Wen).

572 Except for Xiaochuan Fang who is School of Electronic Engineering and Computer Science,
573 Queen Mary University of London, London, United Kingdom, other authors are with the
574 School of Information and Communication Engineering, University of Electronics Science
575 and Technology of China, Chengdu, China; e-mail: wgj@uestc.edu.cn,
576 ligang1986718@163.com

577 **References**

- 578 [1] M. Kim, U. Ha, K. J. Lee, Y. Lee, and H.-J. Yoo, "A 82-nW Chaotic Map True Random Number
579 Generator Based on a Sub-Ranging SAR ADC," *IEEE J. Solid-State Circuits*, vol. 52, no. 7, pp. 1953–
580 1965, Jul. 2017.
- 581 [2] A. Gerosa, R. Bernardini, and S. Pietri, "A fully integrated chaotic system for the generation of truly
582 random numbers," *IEEE Trans. Circuits Syst. I*, vol. 49, no. 7, pp. 993–1000, Jul. 2002.
- 583 [3] A. Alabdulkarim, M. Al-Rodhaan, Y. Tian and A. Al-Dhelaan, "A privacy-preserving algorithm for
584 clinical decision-support systems using random forest," *Computers, Materials & Continua*, vol. 58, no.
585 3, pp. 585–601, 2019.
- 586 [4] Z. Zhou, Q.M. J. Wu, Y. Yang, X. Sun, "Region-level Visual Consistency Verification for Large-Scale
587 Partial-Duplicate Image Search," *ACM Transactions on Multimedia Computing, Communications, and*
588 *Applications*. 16(2), pp, 1-25, 2020
- 589 [5] I. V. Chugunkov, M. A. Ivanov, E. A. Gridneva, and N. Yu. Shestakova, "Classification of pseudo-
590 random number generators applied to information security," in 2017 IEEE Conference of Russian
591 Young Researchers in Electrical and Electronic Engineering (EIconRus), St. Petersburg and Moscow,
592 Russia, 2017, pp. 370–373.
- 593 [6] S. Yasuda, K. Uchida, T. Tanamoto, R. Ohba, and S. Fujita, "Ultra-small physical random number
594 generators based on Si nanodevices for security systems and comparison to other large physical
595 random number generators," in 2003 Third IEEE Conference on Nanotechnology, 2003. IEEE-NANO
596 2003., San Francisco, CA, USA, 2003, vol. 2, pp. 531–534.
- 597 [7] T. Zhang, L. Yi, X. Cui, A. Behl and F. Dong, "RFID based non-preemptive random sleep scheduling
598 in wsn," *Computers, Materials & Continua*, vol. 65, no. 1, pp. 835–845, 2020.
- 599 [8] J. Su, Z. Sheng, A. X. Liu, Z. Fu, C. Huang, "An efficient missing tag identification approach in RFID
600 collisions," *IEEE Transactions on Mobile Computing*, pp. 1-12, 2021.
- 601 [9] Z. Zhou, Y. Mu, Q. M. J. Wu, "Coverless Image Steganography Using Partial-Duplicate Image
602 Retrieval," *Soft Computing*. 23(13), pp: 4927-4938, 2019.
- 603 [10] J. Su, R. Xu, S. Yu, B. Wang, and J. Wang, "Redundant rule detection for software-defined
604 networking," *KSI Transactions on Internet and Information Systems*, vol. 14, no. 6, pp. 2735-2751,
605 2020.
- 606 [11] Pangratz and Weinrichter, "Pseudo-Random Number Generator Based on Binary and Quinary
607 Maximal-Length Sequences," *IEEE Trans. Comput.*, vol. C-28, no. 9, pp. 637–642, Sep. 1979.
- 608 [12] K. Yang, D. Blaauw and D. Sylvester, "An All-Digital Edge Racing True Random Number Generator
609 Robust Against PVT Variations," *IEEE Journal of Solid-State Circuits*, vol. 51, no. 4, pp. 1022-1031,
610 April 2016.
- 611 [13] D. Li, Z. Lu, X. Zou, and Z. Liu, "PUFKEY: A High-Security and High-Throughput Hardware True
612 Random Number Generator for Sensor Networks," *Sensors*, vol. 15, no. 10, pp. 26251–26266, Oct.
613 2015.

- 614 [14] Y. Ma, T. Chen, J. Lin, J. Yang, and J. Jing, "Entropy Estimation for ADC Sampling-Based True
615 Random Number Generators," *IEEE Trans.Inform.Forensic Secur.*, vol. 14, no. 11, pp. 2887–2900,
616 Nov. 2019.
- 617 [15] A. A. Hady, "Duty cycling centralized hierarchical routing protocol with content analysis duty cycling
618 mechanism for wireless sensor networks," *Computer Systems Science and Engineering*, vol. 35, no.5,
619 pp. 347–355, 2020.
- 620 [16] H. Zhu, D. Gao and S. Zhang, "A perceptron algorithm for forest fire prediction based on wireless
621 sensor networks," *Journal of Internet of Things*, vol. 1, no. 1, pp. 25-31, 2019.
- 622 [17] S. Kaur and V. K. Joshi, "Hybrid soft computing technique based trust evaluation protocol for wireless
623 sensor networks," *Intelligent Automation & Soft Computing*, vol. 26, no.2, pp. 217–226, 2020.
- 624 [18] J. Su, R. Xu, S. Yu, B. Wang, and J. Wang, "Idle slots skipped mechanism based tag identification
625 algorithm with enhanced collision detection," *KSII Transactions on Internet and Information Systems*,
626 vol. 14, no. 5, pp. 2294-2309, 2020.
- 627 [19] Z. Li, B. Chang, S. Wang, A. Liu, F. Zeng and G. Luo, "Dynamic Compressive Wide-Band Spectrum
628 Sensing Based on Channel Energy Reconstruction in Cognitive Internet of Things," *IEEE Transactions*
629 *on Industrial Informatics*, vol. 14, no. 6, pp. 2598-2607, June 2018.
- 630 [20] F. Xiao, W. Liu, Z. Li, L. Chen and R. Wang, "Noise-Tolerant Wireless Sensor Networks Localization
631 via Multinorms Regularized Matrix Completion," *IEEE Transactions on Vehicular Technology*, vol.
632 67, no. 3, pp. 2409-2419, March 2018.
- 633 [21] Z. Li, F. Xiao, S. Wang, T. Pei and J. Li, "Achievable Rate Maximization for Cognitive Hybrid
634 Satellite-Terrestrial Networks With AF-Relays," *IEEE Journal on Selected Areas in Communications*,
635 vol. 36, no. 2, pp. 304-313, Feb. 2018.
- 636 [22] A. de la Piedra, F. Benitez-Capistros, F. Dominguez, and A. Touhafi, "Wireless sensor networks for
637 environmental research: A survey on limitations and challenges," in *Eurocon 2013, Zagreb, Croatia*,
638 Jul. 2013, pp. 267–274.
- 639 [23] L. Xu, C. Xu, Z. Liu, Y. Wang and J. Wang, "Enabling comparable search over encrypted data for iot
640 with privacy-preserving," *Computers, Materials & Continua*, vol. 60, no. 2, pp. 675–690, 2019.
- 641 [24] B. D. Reddy, V. V. Kumari, and K. Raju, "A new symmetric probabilistic encryption scheme based on
642 random numbers," in *2014 First International Conference on Networks & Soft Computing*
643 *(ICNSC2014)*, Guntur, Andhra Pradesh, India, Aug. 2014, pp. 267–272.
- 644 [25] L. Jinming, M. Jian, and L. Peiguo, "Design and implement of a MCU based random number
645 generator," in *2016 11th International Conference on Computer Science & Education (ICCSE)*,
646 Nagoya, Japan, Aug. 2016, pp. 945–948.
- 647 [26] C. S. Petrie and J. A. Connelly, "A noise-based IC random number generator for applications in
648 cryptography," *IEEE Trans. Circuits Syst. I*, vol. 47, no. 5, pp. 615–621, May 2000.
- 649 [27] W. T. Holman, J. A. Connelly, and A. B. Dowlatabadi, "An integrated analog/digital random noise
650 source," *IEEE Trans. Circuits Syst. I*, vol. 44, no. 6, pp. 521–528, Jun. 1997.
- 651 [28] Q. Tang, B. Kim, Y. Lao, K. K. Parhi, and C. H. Kim, "True Random Number Generator circuits based
652 on single- and multi-phase beat frequency detection," in *Proceedings of the IEEE 2014 Custom*
653 *Integrated Circuits Conference*, San Jose, CA, USA, Sep. 2014, pp. 1–4.

- 654 [29] N. Nalla Anandakumar, S. K. Sanadhya, and M. S. Hashmi, "FPGA-Based True Random Number
655 Generation Using Programmable Delays in Oscillator-Rings," *IEEE Trans. Circuits Syst. II*, vol. 67,
656 no. 3, pp. 570–574, Mar. 2020.
- 657 [30] N. Fujieda, M. Takeda, and S. Ichikawa, "An Analysis of DCM-based True Random Number
658 Generator," *IEEE Trans. Circuits Syst. II*, pp. 1–1, 2020.
- 659 [31] Y. Liu, R. C. C. Cheung, and H. Wong, "A Bias-Bounded Digital True Random Number Generator
660 Architecture," *IEEE Trans. Circuits Syst. I*, vol. 64, no. 1, pp. 133–144, Jan. 2017.
- 661 [32] M. Bucci, L. Germani, R. Luzzi, A. Trifiletti, and M. Varanono, "A high-speed oscillator-based
662 truly random number source for cryptographic applications on a smartcard IC," *IEEE Trans. Comput.*,
663 vol. 52, no. 4, pp. 403–409, Apr. 2003.
- 664 [33] S. Callegari, R. Rovatti, and G. Setti, "Reconfigurable ADC/True-RNG for Secure Sensor Networks,"
665 in *IEEE Sensors, 2005.*, Irvine, CA, USA, 2005, pp. 1072–1075.
- 666 [34] S. Callegari, R. Rovatti, and G. Setti, "Embeddable ADC-based true random number generator for
667 cryptographic applications exploiting nonlinear signal processing and chaos," *IEEE Trans. Signal
668 Process.*, vol. 53, no. 2, pp. 793–805, Feb. 2005.
- 669 [35] F. Pareschi, G. Setti, and R. Rovatti, "Implementation and Testing of High-Speed CMOS True Random
670 Number Generators Based on Chaotic Systems," *IEEE Trans. Circuits Syst. I*, vol. 57, no. 12, pp.
671 3124–3137, Dec. 2010.
- 672 [36] S. Callegari and G. Setti, "ADCs, Chaos and TRNGs: a Generalized View Exploiting Markov Chain
673 Lumpability Properties," in *2007 IEEE International Symposium on Circuits and Systems*, New
674 Orleans, LA, May 2007, pp. 213–216.
- 675 [37] A. Jayaraj, N. N. Gujarathi, I. Venkatesh, and A. Sanyal, "0.6V-1.2V, 0.22pJ/bit True Random Number
676 Generator Based on SAR ADC," *IEEE Trans. Circuits Syst. II*, pp. 1–1, 2019.
- 677 [38] M. Fabbri and S. Callegari, "Very low cost entropy source based on chaotic dynamics retrofittable on
678 networked devices to prevent RNG attacks," in *2014 21st IEEE International Conference on
679 Electronics, Circuits and Systems (ICECS)*, Marseille, France, Dec. 2014, pp. 175–178.
- 680 [39] S. Callegari, M. Fabbri, and A. Beirami, "Very low cost chaos-based entropy source for the retrofit or
681 design augmentation of networked devices," *Analog Integr Circ Sig Process*, vol. 87, no. 2, pp. 155–
682 167, May 2016.
- 683 [40] F. Kodytek and R. Lorencz, "A Design of Ring Oscillator Based PUF on FPGA," in *2015 IEEE 18th
684 International Symposium on Design and Diagnostics of Electronic Circuits & Systems*, Belgrade,
685 Serbia, Apr. 2015, pp. 37–42.
- 686 [41] M. Majzoobi, F. Koushanfar, and S. Devadas, "FPGA-Based True Random Number Generation Using
687 Circuit Metastability with Adaptive Feedback Control," in *Cryptographic Hardware and Embedded
688 Systems – CHES 2011*, vol. 6917, B. Preneel and T. Takagi, Eds. Berlin, Heidelberg: Springer Berlin
689 Heidelberg, 2011, pp. 17–32.
- 690 [42] X. Xu and Y. Wang, "High Speed True Random Number Generator Based on FPGA," in *2016
691 International Conference on Information Systems Engineering (ICISE)*, Los Angeles, CA, USA, Apr.
692 2016, pp. 18–21.
- 693 [43] I. G. Tarsa, G.-D. Budariu, and C. Grozea, "Study on a true random number generator design for
694 FPGA," in *2010 8th International Conference on Communications*, Bucharest, Romania, Jun. 2010, pp.
695 461–464.

- 696 [44] A. Marghescu, P. Svasta, and E. Simion, "Optimising ring oscillator-based true random number
697 generators concept on FPGA," in 2016 39th International Spring Seminar on Electronics Technology
698 (ISSE), Pilsen, Czech Republic, May 2016, pp. 149–153.
- 699 [45] S. Callegari, R. Rovatti, and G. Setti, "First direct implementation of a true random source on
700 programmable hardware," *Int. J. Circ. Theor. Appl.*, vol. 33, no. 1, pp. 1–16, Jan. 2005.
- 701 [46] T. Stojanovski and L. Kocarev, "Chaos-based random number generators-part I: analysis
702 [cryptography]," *IEEE Trans. Circuits Syst. I*, vol. 48, no. 3, pp. 281–288, Mar. 2001.
- 703 [47] G. Setti, G. Mazzini, R. Rovatti, and S. Callegari, "Statistical Modeling of Discrete-Time Chaotic
704 Processes—Basic Finite-Dimensional Tools and Applications," *PROCEEDINGS OF THE IEEE*, vol.
705 90, no. 5, p. 29, 2002.
- 706 [48] B. Schneier, *Applied Cryptography: Protocols, Algorithms, and Source Code in C*. New York: Wiley,
707 1996, pp. 36-37.
- 708 [49] T. Addabbo, M. Alioto, A. Fort, S. Rocchi, and V. Vignoli, "A feedback strategy to improve the
709 entropy of a chaos-based random bit generator," *IEEE Trans. Circuits Syst. I*, vol. 53, no. 2, pp. 326–
710 337, Feb. 2006.
- 711 [50] "A Statistical Test Suite for Random and Pseudorandom Number Generators for Cryptographic
712 Applications," National Institute for Standards and Technology, Special publication 800-22, 2001.
- 713 [51] MSP430FR58xx, MSP430FR59xx, MSP430FR68xx, and MSP430FR69xx Family User's Guide.
714 Literature Number: SLAU367F October 2012–Revised Jan. 2015.
- 715 [52] Information technology – Radio frequency identification for item management – Part 63: Parameters
716 for air interface communications at 860 MHz to 960 MHz Type C First edition, document,
717 international standard,2013.